Crossover in rescaled-range analysis and power spectra: Measurements and simulations

L. I. Berge, N. Rakotomalala,* J. Feder, and T. Jøssang
Department of Physics, University of Oslo, P.O. Box 1048 Blindern, 0316 Oslo 3, Norway
(Received 20 August 1993)

We have measured and simulated particle flow through a single pore and made comparisons with theory. The simulations are based on an experimental system where particles suspended in an electrolyte are caused to flow by pressure difference through a pore. Each particle in the pore gives rise to a pulse in the measured pore resistance. The pulse height is proportional to the particle volume and the pulse width is given by the particle velocity. In dilute solutions individual particle pulses can be detected and analyzed, but at higher concentrations the pulses start to overlap and the signal looks like noise. Measured and simulated signals are analyzed in terms of Hurst's rescaled range (the R/S analysis, where R is the range and S the standard deviation) and the power spectrum. The signal is sampled and we find a clear crossover from persistent behavior (Hurst exponent $H \simeq 1$) for short times corresponding to the fact that particles reside a finite time in the pore to an independent process ($H \simeq 0.5$) corresponding to the uncorrelated entry of particles into the pore. The calculated effective Hurst exponent depends on the time resolution (sampling interval) used, but R/S curves for different sampling intervals scale when reduced time (sampling interval divided by pulse width) is included in the analysis and yields a nice data collapse for experiments on different types of particles, flow rates, and pore sizes.

PACS number(s): 05.40.+j, 47.15.Pn, 47.60.+i

I. INTRODUCTION

Fractal time series (fractional Brownian motion) have attracted much attention in many fields of science after Mandelbrot's pioneering work (see Refs. [1,2] for a discussion). For a fractal time series one expects power-law scaling of statistical measures on the time series. For the Hurst rescaled-range (R/S) analysis [1–3] one finds for fractional Brownian motion that $R/S \sim \tau^H$, where τ is the lag time over which the range R and the variance S are evaluated. Unfortunately, very large data sets are required to obtain reliable estimates of the Hurst exponent H from R/S (or any other statistical measure). With a more limited data set, spanning only three orders of magnitude in τ, misleading exponents are obtained. In situations where the data contain crossover from one value of H for $\tau \ll \tau_\times$ to another value of H when $\tau \gg \tau_\times$, one is easily misled and only an effective exponent is obtained. We know of only one case where a crossover has been analyzed — the wave-height statistics of ocean waves off the Norwegian coast [4] discussed in Chapter 11 in Ref. [2]. In that case $H \simeq 0.92$ for $\tau < \tau_\times$ and $H \simeq 0.52$ for $\tau > \tau_\times$ with $\tau_\times \simeq 14$ days.

In this paper we discuss experiments and simulations of a simple system that can be easily understood and that exhibits a clear crossover. We show that rescaling the results of different experiments to a common data-collapse plot is a powerful method to use in crossover situations and allows the determination of H both above and below the crossover time. The exponents found are those expected from theory. We also discuss similarities and differences between R/S analysis and the power spectrum when trying to extract information from a fluctuating signal.

The simulations are based on an experimental system: the Coulter principle or the resistive pulse technique [5,6]. Particles suspended in an electrolyte give rise to resistance pulses as they traverse a microscopic pore separating volumes containing the electrodes. In our setup we use long pores (apertures) to ensure a uniform electric and hydrodynamic field inside the pore. This minimizes end effects and the resistive pulses become approximately rectangular. A sequence of overlapping pulses constitutes the noise signal. In our system we have control over all relevant parameters and the underlying process of particle flow through a pore is well understood.

One intriguing aspect of noise signals is that beneath a seemingly erratic appearance information about underlying physical processes exists and can be obtained through appropriate analysis. For ionic systems (similar to our experiments) chemical reaction kinetics has been determined from noise measurements [7] and noise measurements have also been used as a means of counting the number of ions occupying a macroscopic pore [8]. Membrane noise has been an active field of research for many years [9]. Often the noise is analyzed in terms of the correlation function or its Fourier transform — the power spectrum. We find the R/S analysis useful in crossover situations.

*Present address: Université Pierre et Marie Curie, Laboratoire AOMC, boite 78, Tour 13, 4, place Jussieu, 75252 Paris Cedex 05, France.

II. EXPERIMENT

Our experimental setup and its novel features have previously been described [6,10]. Here we briefly recollect the basic features of the experimental system on which the computer simulations are based. The central part of our experimental setup is a cell with two compartments (~ 1 cm^3) connected by a pore. Each compartment contains a silver, silver-chloride electrode. The two electrodes are connected to a constant voltage source. The particles to be analyzed are suspended in an electrolytic solution (0.15M NaCl) which fills the cell. Particles flow through the pore (typically 20 μm in diameter and 200 μm long) driven by a pressure difference. When a particle enters the pore, the momentary increase in electrical resistance of the pore is proportional to the particle volume and the width of the pulse is a measure of the particle transit time through the pore, related to the flow properties [11]. In such a flow system a train of pulses is generated. The degree to which these pulses overlap is determined by the particle concentration, which can easily be varied experimentally.

The pulses were detected using a Keithley model 427 current amplifier with a voltage output. When a particle enters the pore, the pore resistance increases and the current decreases. The output of the current amplifier is an equivalent voltage [6]. In the experiment, the rise time of the signal amplifier and the nonuniformity of the electric field in the entrance and exit regions of the pore give rise to bandwidth limited pulses. The high frequency content of a real pulse is therefore less than for a rectangular pulse, and this shows up in the power spectrum.

III. COMPUTER SIMULATIONS

Figure 1 illustrates two rectangular pulses from two particles passing through a pore and the relevant time variables involved. The basis for the computer simulations is the following: We assume that the particles entering the pore are uncorrelated, i.e., that the time a particle enters the pore, t_i, is independent of previous arrival times. This assumption is valid for dilute solutions, though it may break down for concentrated suspensions (not considered here). The time between the arrival of two particles in the pore (the interevent time), $s_i = t_{i+1} - t_i$, is modeled with a Poisson probability density: $P(s) = \lambda \exp(-\lambda s)$, where the particle rate $\lambda = 1/\bar{s}$. Here $\bar{s}$ is the average time between particles entering the pore.

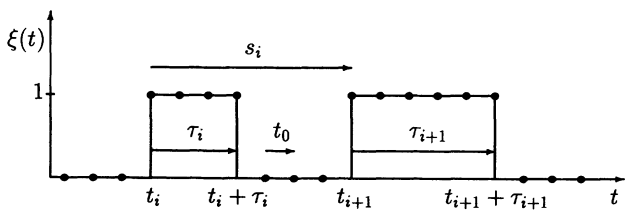

FIG. 1. A portion of a trace showing two rectangular pulses and the relevant times. The filled circles indicate the sampled points. Here t_0 is the sampling interval, $\{t_i\}$ are the arrival times of the pulses, $\{s_i\}$ are the times between the pulses, and $\{\tau_i\}$ are the pulse widths.

We assume that the particle concentration outside the pore is uniform and that there is no redistribution of particles when they enter the pore. However, particles near the pore wall are slower than particles that move near the center of the pore axis, and a distribution of pulse widths results. For small particles in pure Poiseuille flow the pulse width probability density is well approximated by $P(\tau) = A/\tau^3$ [11] [see Eq. (12)], where τ is the pulse width and the normalization constant A depends on particle size. We have used this probability density in the simulations.

A single pulse may be represented by the expression (see Fig. 1)

$$h_i\,(t - t_i) = \begin{cases} 1 & \text{if } t_i \le t \le t_i + \tau_i \\ 0 & \text{otherwise,} \end{cases} \tag{1}$$

where the pulse height has been set equal to 1. For uncorrelated events a sequence of pulses (a trace) can be represented by a superposition of individual pulses:

$$\xi(t) = \sum_i h_i\,(t - t_i)\,. \tag{2}$$

The average number of particles in the pore, $\mathcal{N}$, is related to the particle concentration. The choice of $\mathcal{N}$ determines the degree of overlap of the pulses and can be varied by adjusting $\bar{s} = \bar{\tau}/\mathcal{N}$, where $\bar{\tau}$ is the average pulse width.

The variable parameters used to generate a trace are the average time between pulses, $\bar{s} = 1/\lambda$, and the minimum ($\tau_{\min}$) and maximum ($\tau_{\max}$) pulse width (particle transit time). The ratio of the maximum and minimum pulse width is directly related to the particle size (see Sec. V).

In our simulations the signal length was 16 384 sampled points, where the sampling interval t_0 is the natural time unit. The sampling interval was chosen equal to $\tau_{\min}/25$ or less to get an adequate representation of a rectangular pulse. In Fourier space, this corresponds to a maximum frequency of $655 f_0$, where $f_0 = 1/16\,383 t_0$ is the frequency unit (assuming that the whole interval of time is contained in the range of points given). One should think of the minimum pulse width as being fixed by the experimental situation, while the sampling interval can be varied for a given experiment.

In the simulations the effective particle concentration can be changed by varying the time between pulses. For each generated trace of 16 384 points, the fast Fourier transform (FFT) and power spectrum were calculated using a Parzen window function [12]. The choice of window function was not critical: a square window gave practically the same results. By averaging typically 1000 power spectra we obtained a spectrum with little noise. In order to approach the correct statistics of the underlying process averaging is necessary since there will be fluctuations in the statistics (pulse width distribution and interevent time distribution) of different traces of finite

length. For traces containing a small number of pulses (mostly nonoverlapping), averaging is necessary to obtain a sufficient number of particles, while for traces containing a large number of overlapping pulses, averaging is necessary to separate correlated and uncorrelated events.

Examples of simulated signals are shown in Fig. 2 (10 000 points per trace have been plotted). The upper trace is for an average number of particles in the pore $\mathcal{N} = 9700$, while the other four all have a much lower concentration, corresponding to $\mathcal{N} = 20$. The upper two traces are equivalent except for different particle concentrations. Note that the nature of the noise is not affected by the concentration. The figure illustrates how the appearance of the signal depends on the sampling interval: The four lower traces all correspond to the same experimental situation (the same concentration and minimum pulse width), but probing different frequency regimes. The sampling interval t_0 was varied for each trace as follows (starting from the lower trace): $\tau_{\min}$, $\tau_{\min}/25$, $\tau_{\min}/100$, $\tau_{\min}/1000$, and $\tau_{\min}/1000$, respectively. In all cases, the ratio of the maximum to minimum pulse width was equal to 10. This corresponds to a particle to pore diameter ratio of about 0.05. By changing the time resolution, we can continuously change the noise from approximately white $1/f^0$ to Brownian $1/f^2$. This will be discussed in the following both in terms of R/S analysis and in terms of power spectra.

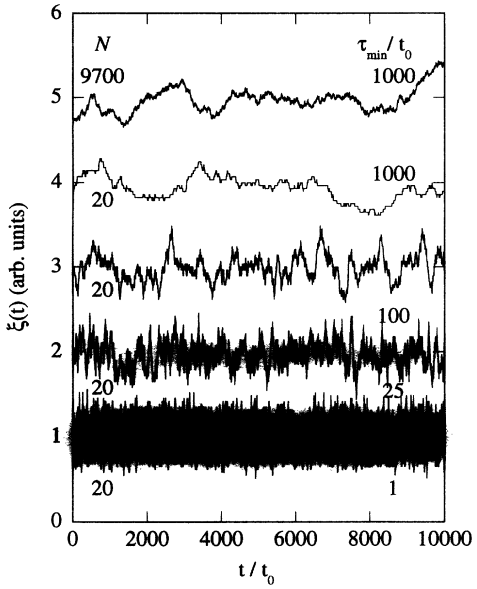

FIG. 2. Examples of simulated traces for varying resolution in time (sampling interval). All traces consist of 10 000 sampled points. The upper trace is for an average number of particles in the pore $\mathcal{N} = 9700$, while the other four all have a much lower concentration, corresponding to $\mathcal{N} = 20$. The sampling interval was varied for each trace as follows (starting from the lower trace): $t_0 = \tau_{\min}$, $t_0 = \tau_{\min}/25$, $t_0 = \tau_{\min}/100$, $t_0 = \tau_{\min}/1000$, and $t_0 = \tau_{\min}/1000$, respectively. The ratio of the maximum to the minimum pulse width was equal to 10 for all cases.

IV. THE HURST EXPONENT

Records in time of various phenomena can be analyzed in terms of Hurst's rescaled range analysis [1,2]. The records are characterized by an exponent H — the Hurst exponent, which can be related to the fractal dimension of the trace of the record. For the R/S analysis of a signal ξ measured with a sampling time t_0 consisting of a total of N_T sampling intervals ($N_T + 1$ points), $\xi(n)$ (at time $t = nt_0$) is divided into smaller independent portions of equal length. Each portion contains N sampling intervals, where $N \leq N_T$. The average of $\xi(n)$ over a time period containing N sampling intervals, $\langle \xi \rangle_N$, is calculated and the standard deviation $S(N)$ of $\xi(n)$ is also calculated for the same time period. The cumulative signal is then calculated:

$$X(n,N) = \sum_{u=1}^{n} [\xi(u) - \langle \xi \rangle_N] \,. \tag{3}$$

The range $R(N)$ is defined as the peak to peak value of $X(n,N)$. Hurst found that the rescaled range, R/S, often is well described by the empirical relation

$$R/S = (N/2)^H \,. \tag{4}$$

For a given time record, R/S is calculated as a function of N. For each value of $N < N_T$, we have several independent estimates of R/S and the final value is the average of all of them. The Hurst exponent H is the slope in a log-log plot, where $0 < H < 1$. For a satistically independent process (Brownian motion) it has been shown [13,14] that $R/S = (\pi N/2)^{1/2}$.

The Hurst exponent can also be related to the exponent β of the power spectrum: $G \sim 1/f^\beta$. An observed signal, $V(t)$, can either be interpreted as the noise itself, $\xi = V$, or as the cumulative signal of an underlying noise process, $X = V$. In the first case $\beta = 2H - 1$ with $-1 < \beta < 1$ and in the second case $\beta = 2H + 1$ with $1 < \beta < 3$ [15,16]. The difference of 2 in the β values comes from integrating the signal in the first case or taking the derivative in the second case. As an example, the cumulative signal of white noise ($\beta = 0$) is Brownian motion ($\beta = 2$). Taking white noise as the noise signal and integrating to determine the range R gives $H = 0.5$ and $\beta = 2H - 1 = 0$. Likewise, taking Brownian motion as the integrated signal and taking the derivative to determine the standard deviation S gives $H = 0.5$ and $\beta = 2H + 1 = 2$. It is not clear how close to the bounds these relations are valid for finite samples of $V(t)$, and care must be taken in their use and interpretations.

We will compare the results of R/S analysis with that of the power spectrum for a case where the frequency dependence varies from $\beta \approx 0$ at low frequencies to $\beta \approx 2$ at high frequencies. The effect of this crossover on the estimated Hurst exponent will be discussed.

V. THE POWER SPECTRUM

The correlation function $C(\tau)$ is defined by [17]

$$C(\tau) = \overline{V(t)V(t+\tau)} \,, \tag{5}$$

where the bar denotes a time average and $V(t)$ is the difference between the current amplifier output voltage and its average value. The autocorrelation function is nonzero over a time span where the events are causally related in the voltage signal, determined by the pulse width τ.

For rectangular particle pulses the autocorrelation function becomes ($\tau \geq 0$)

$$C(\tau) = \sum_k \mathcal{N}_k (\Delta V_k)^2 \left(1 - \frac{\tau}{\tau_k}\right), \quad \tau \leq \tau_{\max}, \tag{6}$$

where $\mathcal{N}_k$, ΔV_k, and τ_k are the average number of particles in the pore, the pulse height, and the pulse width of the kth class of particles. For times longer than the maximum pulse width ($\tau_{\max}$), the autocorrelation function is equal to zero. The sum includes all classes of pulse widths $\tau_k \geq \tau$. This expression can be used, for instance, in the case of electrophoretic particle flow [8] or in the present case, as an approximation to the continuous spread in pulse widths in pure Poiseuille flow. In the case of particles in Poiseuille flow, a class k particle includes all particles having pulse widths in a subinterval about τ_k.

If P_k is the probability of having pulse widths in a subinterval about τ_k, then we have the relation

$$\frac{\mathcal{N}_k}{\mathcal{N}} = P_k \frac{\tau_k}{\overline{\tau}} . \tag{7}$$

Here $\mathcal{N}$ is the average number of particles in the pore, $\mathcal{N} = \sum_k \mathcal{N}_k$, and $\overline{\tau}$ is the average pulse width, $\overline{\tau} = \sum_k P_k \tau_k$. In terms of the probability P_k, the autocorrelation function can now be written

$$C(\tau) = \mathcal{N}(\Delta V)^2 \frac{1}{\overline{\tau}} \sum_k P_k \tau_k \left(1 - \frac{\tau}{\tau_k}\right), \quad \tau \leq \tau_{\max} . \tag{8}$$

It has been assumed that the particles are monodisperse, i.e., $\Delta V_k = \Delta V$. The power spectrum $G(f)$ is the Fourier transform of the autocorrelation function (the Wiener-Khinchin relation) and we obtain

$$G(f) = \mathcal{N}(\Delta V)^2 \frac{1}{\overline{\tau}} \sum_k P_k \tau_k^2 \left(\frac{\sin \pi f \tau_k}{\pi f \tau_k}\right)^2 . \tag{9}$$

The amplitude of the power spectrum is

$$G(0) = \mathcal{N}(\Delta V)^2 \frac{\overline{\tau^2}}{\overline{\tau}} , \tag{10}$$

where $\overline{\tau^2} = \sum_k P_k \tau_k^2$.

The probability of having pulse widths in an interval about τ_k is

$$P_k = \int_{\tau_{k-1/2}}^{\tau_{k+1/2}} P(\tau) d\tau , \tag{11}$$

where we use the fact that the sampled pulse width can only differ in units of t_0, and we have chosen to discretize the width probability density $P(\tau)$ into classes of width t_0. For small particles in pure Poiseuille flow $P(\tau)$ is given by [11]

$$P(\tau) = 2\tau_{\min}^2 \left[1 - \left(\frac{\tau_{\min}}{\tau_{\max}}\right)^2\right]^{-1} \frac{1}{\tau^3} . \tag{12}$$

The minimum pulse width is determined by the maximum fluid flow velocity and the maximum pulse width is essentially determined by the particle size, which limits how close the center of the particle can come to the pore wall where the fluid velocity is zero. The average pulse width is given by

$$\overline{\tau} = 2\tau_{\min} \left(1 + \frac{\tau_{\min}}{\tau_{\max}}\right)^{-1} , \tag{13}$$

and the average of the pulse width squared is

$$\overline{\tau^2} = 2\tau_{\min}^2 \left[1 - \left(\frac{\tau_{\min}}{\tau_{\max}}\right)^2\right]^{-1} \ln \frac{\tau_{\max}}{\tau_{\min}} . \tag{14}$$

The ratio $\tau_{\min}/\tau_{\max} = 1 - x_m^2$, where $x_m = 1 - (d/D)$ is the maximal fractional off-axis displacement of the center position of the particle, valid for small particle sizes. In this model we assume that the particles follow streamlines and do not perturb the flow.

VI. RESULTS AND DISCUSSION

A. Simulations

The appearance of the traces shown in Fig. 2 clearly depends on the time that we choose to sample the signal. This is in contrast to a fractal signal where the appearance does not depend on the resolution. Performing R/S analysis on time records measured with our system showed that the Hurst exponent varied from 0.5 to 1 when the measured trace was taken as the noise signal. This is illustrated in Fig. 3 for three of the simulated

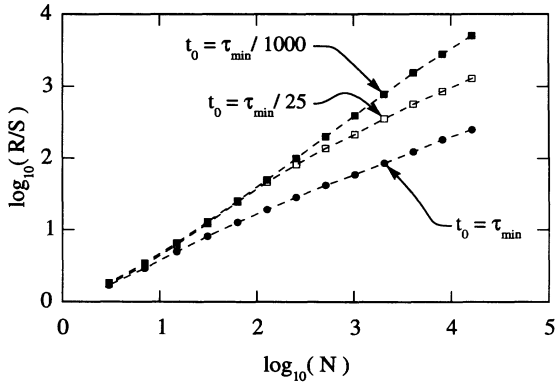

FIG. 3. $\log_{10}(R/S)$ as a function of $\log_{10}(N)$ for three of the simulated traces shown in Fig. 2. For each trace, the points have been connected by dashed lines. The sampling interval was varied for each trace as follows: $t_0 = \tau_{\min}$ (filled circles), $t_0 = \tau_{\min}/25$ (open squares), and $t_0 = \tau_{\min}/1000$ (filled squares). The plotted curves were averaged ten times. Linear fits including all points for each case give average Hurst exponents of 0.58, 0.78, and 0.95, respectively.

traces of Fig. 2. Trying to understand this and its connection to the power spectrum motivated this study to serve as a guide for future experiments.

The resolution in time is determined by the sampling interval t_0 which is the time between two sampled points. Physical time is $t = Nt_0$. By scaling the axes in Fig. 3 with reduced time ($t \to t/\tau_{\min} = Nt_0/\tau_{\min}$), we found a beautiful data-collapse of simulated R/S curves taken in different frequency regimes. Figure 4 shows that the effective Hurst exponent changes when we move from the low frequency to the high frequency regime. The figure shows the same R/S curves as shown in Fig. 3 but with both axes scaled with reduced time, $t_0/\tau_{\min}$. The plotted lines have slopes of 1 and 0.5. We see a clear crossover from the high frequency regime (short times) where the calculated Hurst exponent is close to 1, through an intermediate regime where the relevant flow dynamics takes place, and a low frequency regime (long times) where the Hurst exponent approaches 0.5 (uncorrelated white noise). The crossover time appears to be near $\tau_{\max}$. A similar crossover has previously been observed in wave-height statistics [4].

A Hurst exponent larger than 0.5 implies persistence [2]: an increasing (decreasing) trend in the past implies an increasing (decreasing) trend in the future. Our system should be persistent for times smaller than the maximum transit time: when a particle enters the pore, we know that the signal will be high until the particle exits the pore. The figures illustrate the impact of crossovers in a given system and it shows that the value of the Hurst exponent in such a system will depend on the resolution (sampling interval), unless data-collapse methods are used.

Simulated and theoretical power spectra for a Poisson sequence of rectangular pulses with a pulse width distribution are shown in Fig. 5. The normalized spectrum, $G(f\tau_{\min})/G(0)$ and frequency, $f\tau_{\min}$, are both plotted on a logarithmic scale. The three lower curves show simulations and theory for maximum to minimum pulse width ratios of 100, 10, and 3 (starting from the bottom). The sampling interval $t_0 = \tau_{\min}/25$ for all three cases and the average number of particles in the pore were 98, 18, and 0.25, respectively. The simulated power spectra have all been averaged 1000 times. The agreement between theory and simulations is excellent and involves no adjustable parameters. The deviations at high frequencies are due to the limited number of points (25) used to represent the rectangular pulse. The upper curve shows the theoretical power spectrum for the limiting case of constant pulse width. However, no data collapse is possible for the power spectra since the shape of the spectra changes as the particle size (pulse width) changes.

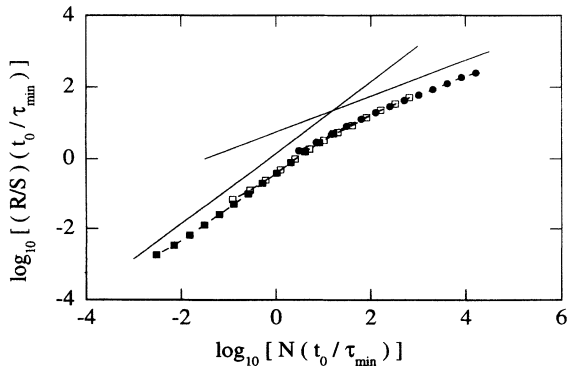

FIG. 4. $\log_{10}[(R/S)(t_0/\tau_{\min})]$ as a function of $\log_{10}[N(t_0/\tau_{\min})]$ for the R/S curves shown in Fig. 2. The lines have slopes equal to 1 and 0.5. Both axes have now been scaled by reduced time to obtain the data collapse.

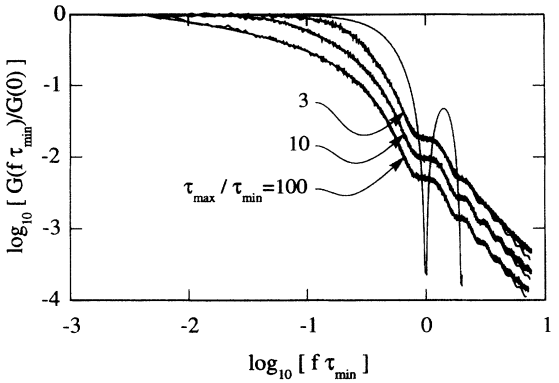

FIG. 5. Simulated and theoretical power spectra for a Poisson sequence of rectangular pulses with a pulse width distribution. The normalized spectrum and frequency have both been plotted on a logarithmic scale. The three lower curves show simulations and theory for maximum to minimum pulse width ratios of 100, 10, and 3 (starting from the bottom). The upper curve shows the theoretical power spectrum for the limiting case of constant pulse width. For the lower curves the deviation between simulations and theory is visible only at high frequencies.

When comparing Figs. 4 and 5 we clearly see the similarities: both figures show a varying frequency dependence. However, the crossover is very slow, and a large frequency range is necessary to clearly see the crossover; Fig. 4 covers effectively seven decades in reduced time. The R/S curve can be obtained without much averaging, which is not true for a good power spectrum. The power spectra are dominated by oscillations in the high frequency regime that stem from the Fourier transform of the square pulses that make up the signal. Since the power spectra do not allow a data collapse we cannot determine reliable scaling exponents for the signals discussed here. A limitation of R/S analysis is that H is restricted between 0 and 1. When using the signal as noise as we have, the upper bound for β is 1, while the signals in our case also contain high frequency components, up to $\beta = 2$. The R/S analysis does not distinguish these higher frequencies well. In terms of the Hurst exponent all β values larger than 1 come out with H close to 1. Close to the bounds it is not clear how to relate the Hurst exponent H to the power spectrum exponent β for sampled signals. So when the Hurst exponent at high frequencies in Fig. 4 saturates close to 1, we cannot determine β correctly. If we instead use the signal as the cumulative signal, covering $1 < \beta < 3$, we find a Hurst exponent close to 0.5 which gives the correct β value in

the high frequency limit.

The power spectrum is a second order statistic whereas R/S is a first order statistic. In practice the R/S analysis is sensitive to long-term trends, but insensitive to high frequency noise.

B. Measurements

R/S analysis has also been performed on measured traces up to 16 384 points in length and sampling intervals from 0.1 ms to 50 ms. Pore and particle sizes have been varied, so have the flow velocity and the time resolution. Results are shown in Fig. 6 where the figure caption gives the experimental parameters for the different curves. The plotted lines have slopes of 1 and 0.5. We again see the nice data collapse of individual R/S curves when the axes are scaled with reduced time. For short times (high frequencies) the slope is close to one as before (Fig. 2). For longer times (smaller frequencies) the slope approaches 0.5. In contrast to the simulations the experiments show an increase in the slope for very long times, indicating that there is some excess noise in the very low frequency regime.

The excess noise in our experiments typically appears around 0.1 Hz, which is quite low (in Ref. [7] only data above 20 Hz were taken). The fact that the same effect appears in an open circuit has led us to believe that it at least partly is due to amplifier noise, since amplifiers normally show some excess noise at low frequencies. We therefore feel that with our present setup it is not trivial to resolve this issue. Possibly excess noise may also be due to very long time correlations in the fluid flow. This is an open question at this stage, but an interesting one. We have, however, not attempted to go into this in the present investigation where we concentrate on crossover phenomena.

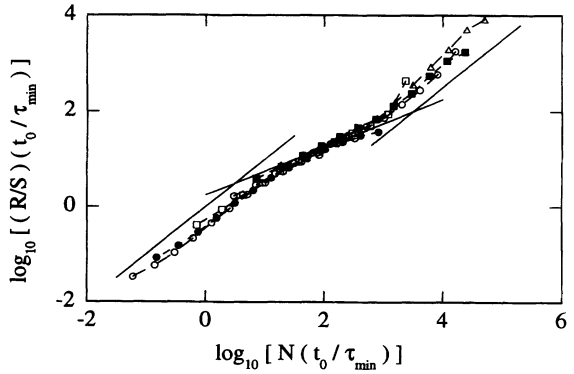

FIG. 6. Data collapse of R/S as a function of N. $\log_{10}[(R/S)(t_0/\tau_{\min})]$ as a function of $\log_{10}[N(t_0/\tau_{\min})]$ for six experimental situations. For each trace, the points have been connected by dashed lines. Open circles: 1 μm diameter spheres flowing through a 27 μm diameter and 540 μm long pore with minimum pulse width equal to 5 ms and sampling intervals 0.1 ms and 5 ms, respectively. Filled circles, same as above except for minimum pulse width equal to 2 ms and sampling interval 0.1 ms. Triangles: ion flow (0.15M NaCl; no particles added to the electrolyte) through the same pore with minimum transit time 13.5 ms and sampling interval 50 ms. Squares: 0.19 μm diameter particles flowing through a 10 μm diameter and 100 μm long pore with minimum pulse width equal to 4.2 ms and sampling intervals 1 ms (filled squares) and 10 ms (open squares).

A comparison between measured and calculated [Eq. (9)] power spectra is shown in Fig. 7. The pore was a cylindrical glass capillary with diameter $D = 70$ μm and length $L = 570$ μm. The particles were monodisperse polystyrene spheres with diameters $d = 3$ μm (lower curves) and 15 μm suspended in 0.15M NaCl in distilled water. The average number of particles in the pore was 460 and 0.27, respectively. A DATA 6000 wave form analyzer (Data Precision Corp., USA) was used to compute and average the power spectra from each measured signal consisting of 4096 points. Both spectra were averaged 400 times. The sampling interval was 0.2 ms and the minimum pulse width 5 ms for both experiments.

We see that the agreement between measurements and theory is quite good. For the 15 μm particles it was necessary to take into account that large particles lag the flow: this increases $\tau_{\max}/\tau_{\min}$ from 2.6 to 3.35 (see Ref. [11] for details) and improves the agreement with theory. Both theoretical curves have been plotted for comparison. The experimental curves lie lower than theory at high frequencies due to the finite rise time of the real pulses.

VII. CONCLUSIONS

We have studied conductance fluctuations due to the presence of particles in a current carrying pore. This system has a crossover in the power spectrum from approximately white noise at low frequencies to $1/f^2$ at high

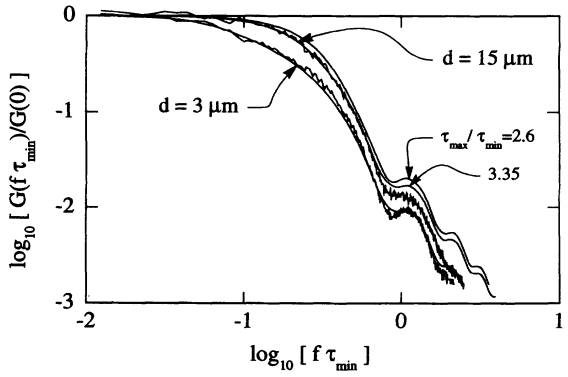

FIG. 7. A comparison between measured and theoretical [based on rectangular pulses: Eq. (9)] power spectra plotted on a logarithmic scale. The two cases are for 15 μm (upper curves) and 3 μm (lower curves) diameter polystyrene spheres flowing through a 70 μm diameter and 540 μm long glass capillary. For the large particles the theoretical curve has been plotted for two values of $\tau_{\max}/\tau_{\min}$: 2.6 and 3.35. The latter corrects for the fact that large particles lag the flow and it clearly gives the best agreement with the experiment. The minimum pulse width was 5 ms and the sampling interval 0.2 ms for both cases.

frequencies. For the power spectrum we find good agreement between simulations, theory, and measurements. However, a data collapse with a clear crossover is not possible. It appears that a well defined model (simulation) is needed in order to interpret the power spectrum. The R/S analysis, on the other hand, allows a data collapse of R/S curves based on time records with different sampling intervals, and different parameters for the experiments. The crossover from persistent behavior ($H \simeq 1$) to independent behavior ($H \simeq 0.5$) is clear both in simulations and in experiments. It is important to be aware that the estimated Hurst exponent will depend on the sampling interval for a system with a crossover for any given time series. Unless data are available for a large dynamical range (i.e., N spans many orders of magnitude) crossover effects dominate, and the effective Hurst exponent tends to be H near 0.75.

The four lowest curves in Fig. 2 represent the same physical situation and differ only in the sampling time t_0. Thus if an experimentalist adjusts the sampling time while watching the resulting time trace on a screen, what sampling time would she choose? $t_0 = \tau_{\min}/1000$ is a too high time resolution and the long-term trends are not properly exhibited in the record. For $t_0 = \tau_{\min}/1$ the trace looks like uninteresting white noise. So a reasonable choice would be in the range $t_0 = \tau_{\min}/100$ to $t_0 = \tau_{\min}/25$. But then, if she is unaware of the underlying crossover from persistent to random behavior, she would fit the resulting R/S curve over a few decades and find an (effective) Hurst exponent of $H \simeq 0.75$ near the average of the H values obtained by Hurst (see Ref. [2]). Thus intuitively one tends to select data that give a nontrivial Hurst exponent and if the crossover is slow the fit may be quite good. We therefore strongly urge the use of data-collapse methods in situations where an external parameter may be varied (the pore length, the pressure difference over the pore, the particle size, and the sampling time in our case) so that crossover phenomena can be discovered.

ACKNOWLEDGMENTS

We are grateful to F. Boger for helpful discussions and for writing the FFT program. We thank E. L. Hinrichsen for letting us use his program for the R/S analysis. This work has been supported by NAVF (Norwegian Research Council for Science and the Humanities), NTNF (Royal Norwegian Council for Scientific and Industrial Research), and VISTA (a research cooperation between the Norwegian Academy of Science and Letters and Statoil).

[1] B. B. Mandelbrot, *The Fractal Geometry of Nature* (W. H. Freeman, San Francisco, 1982).
[2] J. Feder, *Fractals* (Plenum, New York, 1988).
[3] H. E. Hurst, R. P. Black, and Y. M. Simaika, *Long-Term Storage: An Experimental Study* (Constable, London, 1965).
[4] J. Frøyland, J. Feder, and T. Jøssang (unpublished), see Ref. [2].
[5] W. H. Coulter, U.S. Patent No. 2,656,508 (1953).
[6] L. I. Berge, J. Feder, and T. Jøssang, Rev. Sci. Instrum. **60**, 2756 (1989).
[7] G. Feher and M. Weissman, Proc. Natl. Acad. Sci. U.S.A. **70**, 870 (1973).
[8] C. P. Bean and D. C. Golibersuch, in *Electrical Phenomena at the Biological Membrane Level*, edited by E. Roux (Elsevier, Amsterdam, 1977), p. 311.
[9] A. A. Verveen and L. J. DeFelice, Prog. Biophys. Mol. Biol. **28**, 189 (1974).
[10] N. N. Rakotomalala, L. I. Berge, J. Feder, and T. Jøssang, J. Colloid Interface Sci. **148**, 91 (1992).
[11] L. I. Berge, J. Colloid Interface Sci. **135**, 283 (1989).
[12] *Numerical Recipes in C*, 1st ed., edited by W. H. Press, S. A. Teukolsky, W. T. Vetterling, and B. P. Flannery (Cambridge University Press, Cambridge, England, 1988).
[13] H. E. Hurst, Trans. Am. Soc. Civ. Eng. **116**, 770 (1951).
[14] W. Feller, Ann. Math. Stat. **22**, 427 (1951).
[15] R. F. Voss, in *Fundamental Algorithms in Computer Graphics*, edited by R. A. Earnshaw (Springer-Verlag, Berlin, 1985), pp. 805–835, color plates on pp. 13–16.
[16] J. Feder, in *Spontaneous Formation of Space-Time Structures and Criticality*, edited by T. Riste and D. Sherrington (Kluwer Academic Publishers, London, 1991), p. 113.
[17] G. I. Taylor, Proc. London Math. Soc. Ser. 2 **20**, 196 (1920).